micromachines

MDPI

Article

Elasto-Kinematics and Instantaneous Geometric/Kinematic Invariants of Compliant Mechanisms based on Flexure-Hinges

Christian Iandiorio* and Pietro Salvini

Department of Enterprise Engineering, University of Rome "Tor Vergata", Via del Politecnico 1, 00133, Rome, Italy

* Correspondence: christian.iandiorio@uniroma2.it

Abstract: The kinematic synthesis of compliant mechanisms based on flexure-hinges is not an easy task. A commonly used method is to refer to an equivalent rigid model, replacing the flexure-hinges with rigid bars connected with lumped hinges, to use the already known methods of synthesis. This way, albeit simpler, hides some interesting issues. This paper addresses the elasto-kinematics and the instantaneous invariants of flexure-hinges with a direct approach, making use of a nonlinear model to predict their behaviour. The differential equations that govern the nonlinear geometric response are given in a comprehensive form and are solved for flexure-hinges with constant sections. The solution of the nonlinear model is used to obtain an analytical description of two instantaneous invariants: the centre of instantaneous rotation (c.i.r.) and the inflection circle. The main result is that the c.i.r. locations, namely the fixed polode, is not conservative but is loading-path dependent. Consequently, all other instantaneous invariants are loading-path dependents, and the property of instantaneous geometric invariant (i.e. undependent on the motion time-law) can no longer be used. This result is analytically and numerically proved. In other words, it is shown that a careful kinematic synthesis of compliant mechanisms cannot be addressed only considering the kinematics as in rigid mechanisms, but it is essential to take into consideration the applied loads and their histories.

Keywords: Compliant Mechanisms; Instantaneous Invariants; MEMS; Large Displacements; Non-Linear Analysis

Citation: To be added by editorial staff during production.

Academic Editor: Firstname Lastname

Received: date
Revised: date
Accepted: date
Published: date

1. Introduction

In the last two decades, compliant mechanisms [1-3] have produced a growing interest in academic and industrial fields [4,5]. This types of mechanisms manifest their motion through the deformation of some very slender parts [6-8], instead of kinematic pairs. Compliant mechanisms have some advantages if compared to lumped pairs: they do not require lubrication or maintenance inasmuch they have a monolithic form (directly replaceable if failure occurs), they can be made by low-cost additive manufacturing, they are not affected by clearance, friction and wear on contacting parts and they may be very light. These features make them ideal for micro-electro-mechanical systems (MEMS) [9-18] and micro-opto-electromechanical systems (MOEMS) [19-20], precision engineering [21-24], including biological micro-manipulators [25-26], eventually driven by piezoelectric actuators (PEA) [27-30].

On the other hand, the design of compliant mechanisms is tricky; their motion involves large displacements/rotations [31-35] (therefore a high nonlinear geometric behaviour) of the slender joints (flexure hinges), which require to be faced with a nonlinear structural approach. The main challenge regarding the design of these mechanisms is to find consolidated methodologies to define the adequate sizing of flexible joints, such as to realize the required trajectory (kinematic synthesis), but also able to guarantee the desired fatigue life.

The introduction of deformable bodies implies that compliant mechanisms do not depend on a countable number of degrees of freedom (dof) as it is customary for rigid bodies; this dramatically increases the complexity of the design phase [36,37]. For this reason, in literature, many authors make use of pseudo-rigid models [2], in which the compliant behaviour is approximated (strictly for small movements around the reference configuration) using an equivalent rigid mechanism formed by the identified ideal constraints [38,39]. This strategy aims to apply the standard methodologies of kinematic synthesis. Different studies concern this aspect in which the pseudo-rigid model is used for various types of flexure hinges: leaf [40], circular [41], parabolic [42] and notched [43]. The result is that some lumped hinges and flexural springs replace the flexural hinges (the more lumped hinges and springs are used, the more the accuracy increases). Their locations are a function of the geometry of the compliant mechanisms but also of the applied load directions and intensities. Therefore, it is straightforward to observe that the design of compliant mechanisms must be considered a multi-objective problem.

In this paper, we collect, analyze and discuss some important features regarding the design of compliant mechanisms: the elasto-kinematics analysis for some simple configurations as well as the derivation of the instantaneous geometric and kinematic invariants.

2. A comprehensive Analytical model of the Flexure-Hinges Kinematics

A faithful analytical characterization of rigid bodies connected via flexure hinges (Figure 1) should consider that, since the high flexibility of the joints, the configuration changes if the load involves large rotations/displacements of the rigid parts but also the deformable parts (although small strains are assumed) [44-47]. Therefore, it is necessary to involve fully nonlinear models.

Figure 1. Connection of two rigid bodies through a flexure-hinge.

Figure 2 shows a generic 2D flexure-hinge (curvilinear) in two positions. Three reference systems describe the deformed and undeformed configurations along the reference lines; these are parametrized by the curvilinear abscissa s (of the undeformed configuration). The reference systems are: the global (inertial), identified through the orthogonal unit vectors $\boldsymbol{i}_X, \boldsymbol{i}_Y$ (for vector and tensor quantities, bold font is used), and two (local, non-inertial)

mobile frames $\bar{\boldsymbol{e}}_x(s), \bar{\boldsymbol{e}}_y(s)$ and $\boldsymbol{e}_x(s), \boldsymbol{e}_y(s)$, the first associated with the undeformed configuration and the second with the deformed one. Being the motion two dimensional, the unit vector $\boldsymbol{i}_Z = \boldsymbol{i}_X \times \boldsymbol{i}_Y$ is the same for all triads.
The two mobile frames can be expressed in Cartesian components (i.e. by respect to the global frame) through the change-of-basis orthogonal tensors $\boldsymbol{\Lambda}^{\vartheta}, \boldsymbol{\Lambda}^{\psi}$ as follow:

$$\bar{\boldsymbol{e}}_i(s) = \boldsymbol{\Lambda}_{\vartheta} \cdot \boldsymbol{i}_i \tag{1}$$

$$\boldsymbol{e}_i(s) = \boldsymbol{\Lambda}_{\psi} \cdot \boldsymbol{i}_i \tag{2}$$

Where the subscript i is used in place of X, Y or x, y.

$$\boldsymbol{\Lambda}_{\vartheta}(s) = \bar{\boldsymbol{e}}_x \otimes \boldsymbol{i}_X + \bar{\boldsymbol{e}}_y \otimes \boldsymbol{i}_Y = \tag{3}$$

$$= \cos\vartheta \;\boldsymbol{i}_X \otimes \boldsymbol{i}_X - \sin\vartheta \;\boldsymbol{i}_X \otimes \boldsymbol{i}_Y + \sin\vartheta \;\boldsymbol{i}_Y \otimes \boldsymbol{i}_X + \cos\vartheta \;\boldsymbol{i}_Y \otimes \boldsymbol{i}_Y$$

$$\boldsymbol{\Lambda}_{\psi}(s) = \boldsymbol{e}_x \otimes \boldsymbol{i}_X + \boldsymbol{e}_y \otimes \boldsymbol{i}_Y = \tag{4}$$

$$= \cos\psi \;\boldsymbol{i}_X \otimes \boldsymbol{i}_X - \sin\psi \;\boldsymbol{i}_X \otimes \boldsymbol{i}_Y + \sin\psi \;\boldsymbol{i}_Y \otimes \boldsymbol{i}_X + \cos\psi \;\boldsymbol{i}_Y \otimes \boldsymbol{i}_Y$$

The angles $\vartheta(s), \psi(s)$ are shown in Figure 2.

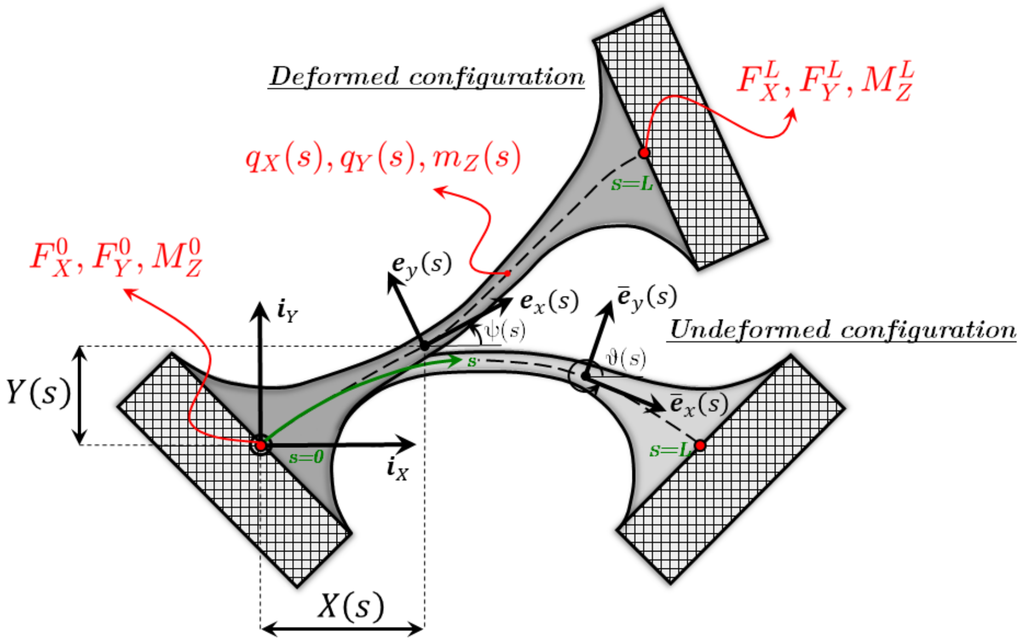

Figure 2. Generic undeformed and deformed configurations.

Based on the previous equations, it is possible to define the curvatures of the reference lines, important intrinsic quantities that characterize the configuration. Applying the derivative of the eq.s(1,2) by respect to s and using again eq.s(1,2) to express the results in the mobile frames $\boldsymbol{e}_x(s), \boldsymbol{e}_y(s)$, they turn out:

$$\frac{d\bar{\boldsymbol{e}}_i(s)}{ds} = \bar{\boldsymbol{K}} \cdot \boldsymbol{e}_i = \bar{\boldsymbol{k}} \times \boldsymbol{e}_i \tag{5}$$

$$\frac{d\boldsymbol{e}_i(\boldsymbol{s})}{ds} = \boldsymbol{K} \cdot \bar{\boldsymbol{e}}_i = \boldsymbol{k} \times \bar{\boldsymbol{e}}_i \tag{6}$$

in which:

$$\overline{\boldsymbol{K}}(s) = \frac{\partial \boldsymbol{\Lambda}_{\vartheta}}{\partial s} (\boldsymbol{\Lambda}_{\vartheta})^T \tag{7}$$

$$\boldsymbol{K}(s) = \frac{\partial \boldsymbol{\Lambda}_{\psi}}{\partial s} \left(\boldsymbol{\Lambda}_{\psi}\right)^{\boldsymbol{T}} \tag{8}$$

are the curvature tensors of the undeformed and deformed reference lines, respectively. The terms in eq.s(7,8) are skew-symmetric tensors (Appendix A); therefore, it is possible to simplify eq.s(5,6) using the curvature vectors, which are the axial vectors of the skew-symmetric curvature tensors:

$$\overline{\boldsymbol{k}}(s) = \frac{d\vartheta}{ds}\, \boldsymbol{i}_Z \tag{9}$$

$$\boldsymbol{k}(s) = \frac{d\psi}{ds}\, \boldsymbol{i}_{\boldsymbol{Z}} \tag{10}$$

A one-dimensional model is adopted; therefore, for each point, the motion that occurs during the configuration change is due to two translations components along $\boldsymbol{e}_x, \boldsymbol{e}_y$, and a cross-section rotation, assumed transversely rigid [48]. This allows to separately examine the axial (ε), shear (γ) and rotational (χ) strains. Adopting a Lagrangian approach, the radius vector which identifies the reference line of the deformed configuration is (Figure 2):

$$\boldsymbol{r}(s) = X\, \boldsymbol{i}_X + Y\, \boldsymbol{i}_Y \tag{11}$$

where $X(s), Y(s)$ are the position of the generic point of the deformed configuration by respect to the global reference system, only functions of the curvilinear abscissa s of the undeformed configuration.
The prime derivative of $\boldsymbol{r}$ is close to $\boldsymbol{e}_x$, but the two vectors differ due to axial and shear strain:

$$\frac{d\boldsymbol{r}(s)}{ds} = (1+\varepsilon)\boldsymbol{e}_x + \gamma\, \boldsymbol{e}_y = \frac{\partial X}{\partial s}\boldsymbol{i}_X + \frac{\partial Y}{\partial s}\boldsymbol{i}_Y \tag{12}$$

Using the reverse of the eq.(2), namely $\boldsymbol{i}_i = \left(\boldsymbol{\Lambda}_{\psi}\right)^T \cdot \boldsymbol{e}_i(s)$, to express the right side of the eq.(12) by respect to the mobile frame, the following relations occur:

$$\varepsilon(s) = \frac{dX}{ds}\cos\psi + \frac{dY}{ds}\sin\psi - 1 \tag{13}$$

$$\gamma(s) = -\frac{dX}{ds}\sin\psi + \frac{dY}{ds}\cos\psi \tag{14}$$

For slender structures, i.e. when the ratio between the half of thickness and the curvature radius is $\ll 1$ [49,50], the rotational strain is:

$$\chi(s) = \left(\boldsymbol{k} - \overline{\boldsymbol{k}}\right)\cdot \boldsymbol{i}_Z = \frac{d\psi}{ds} - \frac{d\vartheta}{ds} \tag{15}$$

Therefore, the Green-Lagrange strains are given by:

$$\varepsilon_x(s,\xi) = \varepsilon - y\chi \tag{16}$$

$$\gamma_{xy}(s) = \gamma \tag{17}$$

where y is the coordinate along $\boldsymbol{e}_y$ that identify the points on the cross-section.
Assuming that the beam is made of an isotropic elastic material, the stress components are: $\sigma_x = E\varepsilon_x$, $\tau_{xy} = G\gamma_{xy}$, where E, G are the axial end shear moduli of elasticity.
In this one-dimensional model, the flexure hinge exchanges forces and moments with the rigid bodies it connects through its ends. For convenience, the load quantities are referred

to the global reference system. At $s = 0$, the force and moment vectors $\boldsymbol{F}_0 = F_X^0\, \boldsymbol{i}_X + F_Y^0\, \boldsymbol{i}_Y$, $\boldsymbol{M}_0 = M_Z^0\, \boldsymbol{i}_Z$ are applied, while in $s = L$ act, the loads $\boldsymbol{F}_L = F_X^L\, \boldsymbol{i}_X + F_Y^L\, \boldsymbol{i}_Y$, $\boldsymbol{M}_L = M_Z^L\, \boldsymbol{i}_Z$. Along the length of the flexure-hinge can also act translational and rotational distributed loads $\boldsymbol{q}(s) = q_X(s)\, \boldsymbol{i}_X + q_Y(s)\, \boldsymbol{i}_Y$, $\boldsymbol{m}(s) = m_Z(s)\, \boldsymbol{i}_Z$. It is worth pointing out that distributed loads are usually omitted in the studies regarding flexure-hinges, as most of the forces are exchanged at the extremes. In this treatment, we include these types of loads because there are some applications in which compliant mechanisms are driven using a distribution of smart materials (e.g. distributed piezoelectric actuators [51] or shape memory alloys [52]); in these cases, the effects of smart-material-based actuators can manifest as distributed loads.

At a generic point s, forces and moment $\boldsymbol{F}(s) = F_X(s)\boldsymbol{i}_X + F_Y(s)\boldsymbol{i}_Y$, $\boldsymbol{M}(s) = M_Z(s)\boldsymbol{i}_Z$ result. Imposing that the flexure-hinge respects the equilibrium in the deformed configuration, forces and moment at the generic curvilinear abscissa s can be expressed as a function of the applied loads [53]. Assuming $\boldsymbol{F}_0, \boldsymbol{M}_0$ the following equations results:

$$F_X(s) = -F_X^0 - \int_0^s q_X(\tilde{s})\, d\tilde{s} \tag{18}$$

$$F_Y(s) = -F_Y^0 - \int_0^s q_Y(\tilde{s})\, d\tilde{s} \tag{19}$$

$$M_Z(s) = -M_Z^0 - YF_X^0 + XF_Y^0 + \int_0^s \left[\left(\tilde{Y} - Y\right)q_X(\tilde{s}) - \left(\tilde{X} - X\right)q_Y(\tilde{s}) - m_Z(\tilde{s})\right] d\tilde{s} \tag{20}$$

where $X(s), Y(s)$ depend on s, while $\tilde{X}(\tilde{s}), \tilde{Y}(\tilde{s})$ on the dummy variable $\tilde{s}$.

Appendix B shows the eq.s(18-20) when known forces and moment $\boldsymbol{F}_L, \boldsymbol{M}_L$ are given at $s = L$, and makes explicit the relations between $\boldsymbol{F}_0, \boldsymbol{M}_0$ and $\boldsymbol{F}_L, \boldsymbol{M}_L$.

The axial and shear internal forces $N(s), T(s)$ act in the normal and orthogonal direction of the cross-section, that is counterclockwise rotated of the small angle γ by respect to the mobile frame $\boldsymbol{e}_x, \boldsymbol{e}_y$. The shear distortion effect on the direction of the internal forces can be neglected, obtaining: $\boldsymbol{N}(s) = (N - \gamma T)\, \boldsymbol{e}_x + (T + \gamma N)\, \boldsymbol{e}_y \cong N\, \boldsymbol{e}_x + T\, \boldsymbol{e}_y$. Therefore, the internal forces $\boldsymbol{N}(s)$ can be obtained from $\boldsymbol{F}(s)$ using eq.(2):

$$\boldsymbol{N}(s) = \boldsymbol{\Lambda}_\psi \cdot \boldsymbol{F}(s) \tag{21}$$

or, in components:

$$N(s) = F_X(s)\cos\psi + F_Y(s)\sin\psi \tag{22}$$

$$T(s) = -F_X(s)\sin\psi + F_Y(s)\cos\psi \tag{23}$$

Due to the planar motion, the internal moment is simply $\boldsymbol{M}(s) = M_z(s)$.

Being $\boldsymbol{\sigma}(s,\xi) = \sigma_x\, \boldsymbol{e}_x \otimes \boldsymbol{e}_x + \tau_{xy}\left(\boldsymbol{e}_x \otimes \boldsymbol{e}_y + \boldsymbol{e}_y \otimes \boldsymbol{e}_x\right)$ the stress tensor (having neglected the shear distortion effect again), the internal forces and moment $\boldsymbol{N}(s), \boldsymbol{M}(s)$ can be expressed as the integration along the cross-section of the stress vector $\boldsymbol{t} = \boldsymbol{\sigma} \cdot \boldsymbol{e}_x = \sigma_x\, \boldsymbol{e}_x + \tau_{xy}\, \boldsymbol{e}_y$:

$$\boldsymbol{N}(s) = \int_A \boldsymbol{t}\, dA \quad ; \quad \boldsymbol{M}(s) = \int_A \left(y\, \boldsymbol{e}_y\right) \times \boldsymbol{t}\, dA \tag{24}$$

From which, using eq.s(16,17) and assuming the local reference as principal of inertia and with the origin on the barycenter of the section, the forces-strains relationships are:

$$N(s) = EA\varepsilon \quad ; \quad T(s) = GA_s\gamma \quad ; \quad M(s) = EI\chi \tag{25}$$

where $A(s), I(s)$ are the area and moment of the inertia of the cross-section, and $A_s(s)$ is the effective shear area [48,54].
The three unknows that identify the deformed configuration are X, Y, ψ; they can be found applying the eq.s(22,23,25) in the eq.s(13-15):

$$\frac{dx}{ds} = \cos\psi + \left(\frac{\cos^2\psi}{EA} + \frac{\sin^2\psi}{GA_s}\right)F_X(s) - \left(\frac{1}{GA_s} - \frac{1}{EA}\right)\sin\psi\cos\psi\, F_Y(s) \tag{26}$$

$$\frac{dy}{ds} = \sin\psi - \left(\frac{1}{GA_s} - \frac{1}{EA}\right)\sin\psi\cos\psi\, F_X(s) + \left(\frac{\sin^2\psi}{EA} + \frac{\cos^2\psi}{GA_s}\right)F_Y(s) \tag{27}$$

$$\frac{d\psi}{ds} = \frac{d\vartheta}{ds} + \frac{M(s)}{EI} \tag{28}$$

The eq.s(26-28) form a nonlinear first-order ODE system and holds for every type of flexure-hinges (with variable section, initially curvilinear, etc.). It is not possible to solve them analytically in a general form (i.e. for all types of load conditions) [31,33,45]. The boundary conditions (b.c.) on the eq.(26,27) are trivial, i.e. $X(s=0) = X_0$, $Y(s=0) = Y_0$, namely the choice of the location of the global reference system. More interesting are the b.c. of the eq.(28), which represents the difficulties encountered in solving this system; in general, $\psi(s=0) = \psi_0$ is unknown, but above all, it is unknown the bending moment M_Z^0 at the origin (namely, the curvature $\psi'(s=0) = \psi'_0$). The b.c. regarding the bending moment can usually be known at the end $s = L$ (e.g. the case of a cantilever beam loaded by concentrated forces at the end), and this entails that the b.c. problem becomes a boundary value problem (b.v.p.). As it is well known, the numerical methods to solve ODE only work with initial value problems (i.v.p.); therefore, to solve a b.v.p., a shooting method should be adopted [31,33] that involves integrating several times the systems (26-28).
Often the eq.(28) appears as a second-order ODE; applying the derivative of eq.(28), being careful to use the Leibniz integration rule (differentiation under the integral sign) for the derivative of the eq.(20), one obtains:

$$\frac{d^2\psi}{ds^2} + \left(\frac{1}{EI}\frac{d^2EI}{ds^2}\right)\frac{d\psi}{ds} = \frac{d^2\vartheta}{ds^2} + \frac{1}{EI}\left[\left(\frac{d\,EI}{ds}\right)\frac{d\vartheta}{ds} + \frac{dy}{ds}F_X(s) - \frac{dx}{ds}F_Y(s) + m_z\right] \tag{29}$$

This form does not change the aforementioned difficulties; the unknows remain ψ'_0 and ψ_0, but the form of the eq.(29) can be analytically integrated in some cases that will be used in the following to provide some benchmark results regarding the computation of the fixed and mobile polodes of compliant mechanisms.
Furthermore, it is important to emphasize (for what follows) that in compliant mechanism applications, the forces and moments are not directly applied at the flexure-hinges ends but along the rigid bodies connected with it. In this case, the forces and moments F_X^0, F_Y^0, M_Z^0 or F_X^L, F_Y^L, M_Z^L applied to the flexure-hinge are also function of the unknows angles ψ_0 or ψ_L. Consider Figure 3, where a flexure-hinge connects two rigid bodies, of which the one on the left is clamped. The rigid body on the right is loaded at point P with the forces and moment $\boldsymbol{F}_P = F_X^P\,\boldsymbol{i}_X + F_Y^P\,\boldsymbol{i}_Y$, $\boldsymbol{M}_P = M_Z^P\,\boldsymbol{i}_Z$. Applying the static equivalence, the forces and moment F_X^L, F_Y^L, M_Z^L experienced by the flexure-hinge are not only a function of known quantities as F_X^P, F_Y^P, M_Z^P and x_P, y_P, but also by the unknow angle ψ_L (or ψ_0):

$$F_X^L = F_X^P \tag{30}$$

$$F_Y^L = F_Y^P \tag{31}$$

$$M_Z^L = M_Z^P + \left[x_P\, \boldsymbol{e}_x(L) + y_P\, \boldsymbol{e}_y(L)\right] \times (F_X^P\ \boldsymbol{i}_X + F_Y^P\ \boldsymbol{i}_Y) = \tag{32}$$

$$= M_Z^P + (x_P \cos\psi_L - y_P \sin\psi_L)\, F_Y^P - (x_P \sin\psi_L - y_P \cos\psi_L)\, F_X^P$$

Therefore, as previously mentioned, in this scenario the applied moment M_Z^L depends on the unknow angle ψ_L.
This case is an example in which the b.c. are a b.v.p., inasmuch the moment M_Z^0 at the origin is unknown, but it must be found such that at the end of the computation the final moment M_Z^L obtained from the curvature $\psi'(L)$ respects eq.(32). In the following section, some analytical solution of eq.s(26-28) are presented under some simplifying assumption.

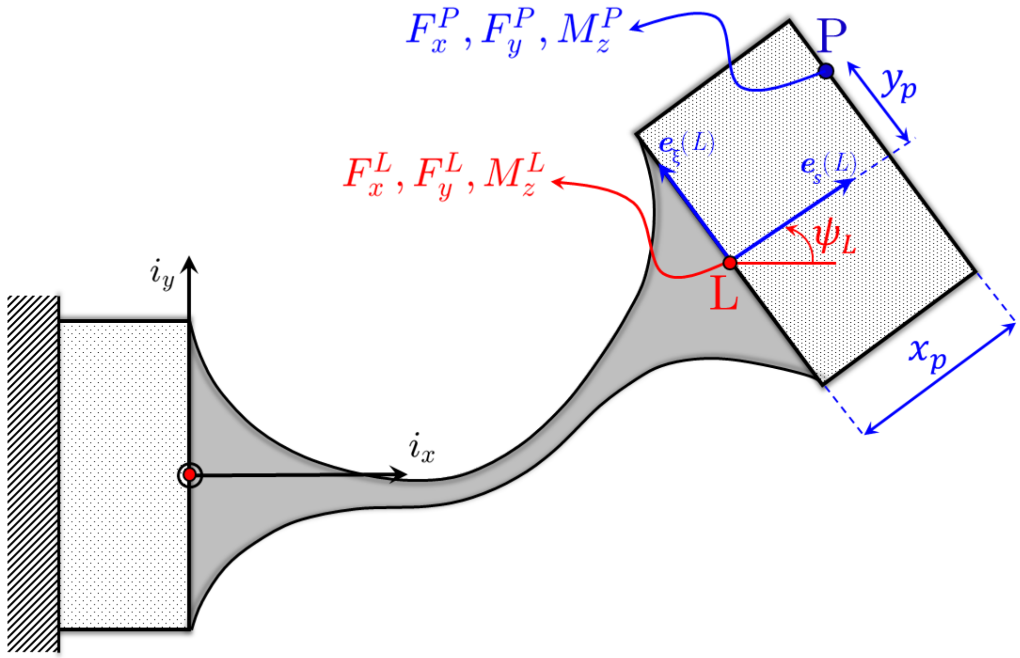

Figure 3. Flexure-hinge loaded by forces and moment applied in a generic point of the rigid body connected with it.

2.1. Analytical solution

An analytical solution of the eq.s(26,27,29) can be found taking into account some assumptions: the extensional and shear strains are negligeble ($\varepsilon = \gamma = 0\ or\ EA, GA_s \to \infty$), the section has a constant shape ($EI = const.$), the initial curvature is constant ($\vartheta' = const.$) and the distributed loads are null ($q_X = q_Y = m_Z = 0$). Although the analytical solution requires the assumption of a constant section, this is a valuable solution, inasmuch for notched flexure-hinges the main deformable part is the central ones with constant section [63] (Figure 3).
Under these conditions, the forces F_X, F_Y (eq.s(18,19 or B1,B2)) acting at a generic point s are constant, and the eq.s(26,27,29) becomes:

$$\frac{dX}{ds} = \cos\psi \tag{33}$$

$$\frac{dY}{ds} = \sin\psi \tag{34}$$

$$EI\,\frac{d^2\psi}{ds^2} = F_X \sin\psi - F_Y \cos\psi \tag{35}$$

Multiplying both sides of the latter equation by ψ', eq.(35) can be integrated, obtaining:

$$\frac{EI}{2}\left(\frac{d\psi}{ds}\right)^2 = c - F_X\cos\psi - F_Y\sin\psi \tag{36}$$

where c is an integration constant; if b.c. at $s = 0$ are applied:

$$c = F_X\cos\psi_0 + F_Y\sin\psi_0 + \frac{EI}{2}\left(\vartheta' + \frac{M_Z^0}{EI}\right)^2 \tag{37}$$

otherwise, if b.c. at $s = L$ are applied:

$$c = F_X\cos\psi_L + F_Y\sin\psi_L + \frac{EI}{2}\left(\vartheta' + \frac{M_Z^L}{EI}\right)^2 \tag{38}$$

Eq.(36) can be rearranged as follows:

$$\frac{d\psi}{ds} = sign(\psi')\, f(\psi) \tag{39}$$

in which:

$$f(\psi) = \sqrt{\frac{2}{EI}(c - F_X\cos\psi - F_Y\sin\psi)} \tag{40}$$

The function $sign(\psi')$ is unknown and generally piecewise defined; it defines the sign of the curvature. This is a crucial point; being the ODE system in eq.(33-35) nonlinear, more than one solution generally exist. These multiple possible solutions of the deformed shape have an unknown number of inflection points (i.e. points where the curvature $\psi' = 0$, and therefore the sign of the curvature changes). Furthermore, the presence of one or more inflection points depends on the position of the applied load in the deformed (unknown) configuration. A priori determination of the distribution of inflection points (i.e. the exact determination of $sign(\psi')$) as only function of the magnitude of the applied loads is, until now, an open problem. We will not deal with that in the following, but we present the solution limited to at most 1 inflection point.

If no internal inflection points are present, the angle $\psi(s)$ is monotone and the sign function is trivial:

$$sign(\psi') = \pm 1 \quad \forall \quad \psi(s) \in (\psi_0, \psi_L) \tag{41}$$

but the latter can be zero at the extremities if the terms $\left(\vartheta' + \frac{M_Z^0}{EI}\right)$ or $\left(\vartheta' + \frac{M_Z^L}{EI}\right)$ are nulls in ψ_0 or ψ_L.

If an inflection point exists, eq.(39) is null at a point s_{in} , which corresponds to an angle $\psi(s = s_{in}) = \psi_{in}$:

$$F_X\cos\psi_{in} + F_Y\sin\psi_{in} = c \tag{42}$$

Latter equations can be manipulated to obtain a relation between the angle ψ_{in} and the triplet $\psi_0, \vartheta', M_Z^L$ or $\psi_L, \vartheta', M_Z^0$, respectively if the eq.(37) or (38) is chosen for c:

$$\psi_{in} = \arcsin\left(\frac{c}{\sqrt{{F_X}^2 + {F_Y}^2}}\right) - \varphi \tag{43}$$

where:

$$\varphi = \mathrm{atan2}(F_Y, F_X) \tag{44}$$

The authors suspect that if multiple inflection points $\psi_{in,1}, \psi_{in,2}, \dots, \psi_{in,k}$ exists, the relation between the generic inflection-point angle $\psi_{in,k}$ and the angle ψ_0 or ψ_L, can always be found with the eq.(42), but the sign-equation and the closure equation (eq.(46)) must

be subdivided into parts. This issue has not yet been thoroughly investigated, and it is beyond the scope of the present paper.
The sign function for a single inflection point appears in a more articulated form than eq(41), namely as a piecewise-defined function:

$$sign(\psi') = \begin{cases} sign(\psi_0') & if \quad \psi(s) \in (\psi_0, \psi_i) \\ 0 & if \quad \psi(s) = \psi_i \\ sign(\psi_L') & if \quad \psi(s) \in (\psi_i, \psi_L) \end{cases} \tag{45}$$

where $sign(\psi_0')$, $sign(\psi_L')$ are constant values that can be ± 1, and again eq.(45) can be zero at the extremities if the terms $\left(\vartheta' + \frac{M_Z^0}{EI}\right)$ or $\left(\vartheta' + \frac{M_Z^L}{EI}\right)$ are nulls in ψ_0 or ψ_L.
Both in the case of zero or a single inflection point, the determination of ψ_{in} is conditioned by the knowledge of ψ_0 or ψ_L. To find the latter, still unknown, it is necessary to continue the integration of eq.(39), obtaining:

$$L = \int_{\psi_0}^{\psi_L} \frac{sign(\psi')\, d\psi}{f(\psi)} \tag{46}$$

Eq.(46) appears as a closure equation which involves only geometric variables and applied loads; it is not possible to integrate analytically eq.(46), and the search for the unknown parameter $(\psi_0 \; or \; \psi_L)$ involves an attempt method [44,45]. It is important to observe that the function $f(\psi)$ also depends on ψ_L.
Once solved the eq.(46) with the considered geometry and loads, the deformed shape can be obtained through the integration of the eq.s(33,34), using the relation $ds = d\psi/\psi'$, applying the eq.(39) and the b.c. $X_0 = X(s=0)$, $Y_0 = Y(s=0)$:

$$X(\psi) = X_0 + \int_{\psi_0}^{\psi} \frac{sign(\tilde{\psi}') \cos \tilde{\psi}}{f(\tilde{\psi})} d\tilde{\psi} \tag{47}$$

$$Y(\psi) = Y_0 + \int_{\psi_0}^{\psi} \frac{sign(\tilde{\psi}') \sin \tilde{\psi}}{f(\tilde{\psi})} d\tilde{\psi} \tag{48}$$

where $\tilde{\psi}$ is a dummy variable and $\psi(s) \in [\psi_0, \psi_L]$
Similarly to eq.(46), it is not possible to integrate analytically eq.s(47,48), which require of a numerical integration to be computed. However, eq.s(46-48) are computationally advantageous if compared to a full-length numerical integration required to compute eq.s(26-28); this is because eq.s(46-48) allows computing the results also on a single point (e.g. the end point), which is very advantageous in the computation of the instantaneous invariants which are treated in the following section.
If an inflection point exists, eq.s(46-48) involve improper integrals. To avoid complications due to singularity, eq.s(46-48) are evaluated by applying a trick reported in Appendix C.

3. Instantaneous Geometric and Kinematic Invariants for compliant mechanism

The kinematic synthesis of rigid planar mechanisms is often performed using instantaneous geometric and kinematic invariants [55-59]. The first types of invariants (geometric) are more useful, as they have the important property of being independent of the motion time-law. They include important geometric loci, such as the fixed and mobile polodes (and their curvature, appearing in the Euler-Savary formula), the first Bresse's circle (zero normal acceleration), the cubic curve of stationary curvature, the Ball's point and the Burmester points. The second types (kinematic) define instantaneous properties of the motion but are a function of the motion time-law (i.e. angular velocity, acceleration etc.). Some examples of instantaneous kinematic invariants are the second Bresse's circle (zero tangential acceleration), the centre of the accelerations (i.e. the point with null acceleration, the intersection between the first and second Bresse's circles, other than the centre of instantaneous rotation), the jerk and Javot centres, etc.

The instantaneous invariants, mainly geometric ones, are essential to set in analytical form problems of kinematic synthesis [59-62].

At the best literature knowledge of the authors, for compliant mechanisms, the instantaneous invariants are not yet used with their analytical form. As mentioned in §1, pseudo-rigid models commonly are used [2,38,39] in which the flexure-hinges are replaced by rigid bars connected with lumped hinges. However, this approach implies that the bar lengths and the positions of the lumped hinges must be changed during the motion as the centre of instantaneous rotation moves, and their positions change as a function of the applied load.

In this section, the determination of the instantaneous invariants is addressed with a direct approach, considering the real deformable behaviour of flexure-hinges.

The first instantaneous geometric invariant investigated is the centre of instantaneous rotation. In order to study the relative motion, the case of a flexure hinge connected with a fixed and a mobile rigid body is taken into account. The position of a generic point M of the mobile rigid body in Figure 4 is:

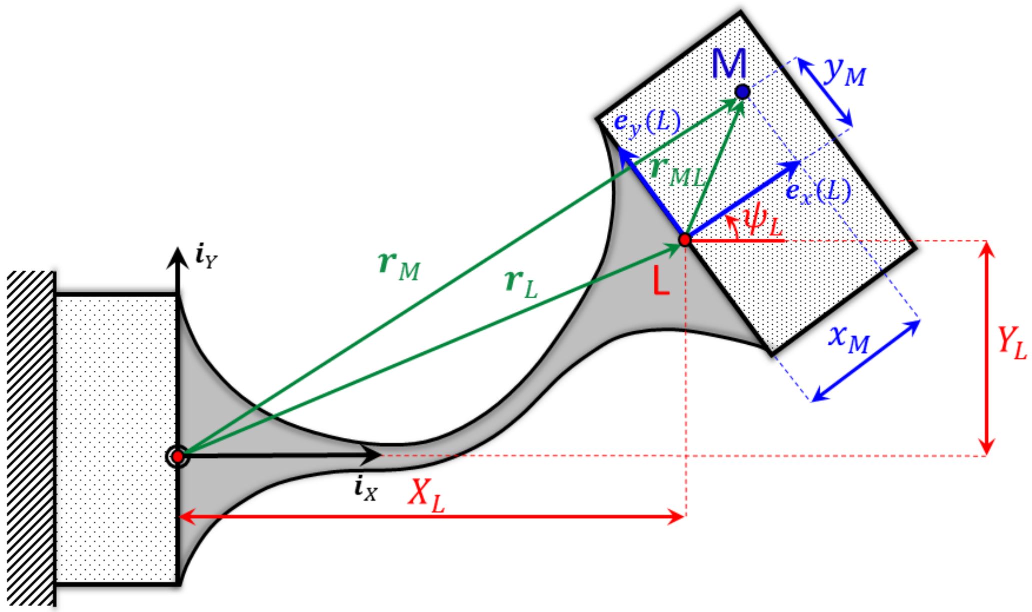

Figure 4. Generic configuration of two rigid bodies (fixed and mobile) connected by a flexure-hinge

$$\boldsymbol{r}_M = \boldsymbol{r}_L + \boldsymbol{r}_{ML} \tag{49}$$

where:

$$\boldsymbol{r}_M = X_M\, \boldsymbol{i}_X + Y_M\, \boldsymbol{i}_Y \tag{50}$$

$$\boldsymbol{r}_L = X_L\, \boldsymbol{i}_X + Y_L\, \boldsymbol{i}_Y \tag{51}$$

$$\boldsymbol{r}_{ML} = x_M\, \boldsymbol{e}_x(L) + y_M\, \boldsymbol{e}_y(L) = \boldsymbol{\Lambda}_{\psi_L} \cdot \boldsymbol{x}_{ML} \tag{52}$$

in which eq.(2) has been used in eq.(52). The others terms that appear in eq.s(51,52) are: $X_L = X(\psi = \psi_L)$, $Y_L = Y(\psi = \psi_L)$, $\boldsymbol{x}_{ML} = x_M\, \boldsymbol{i}_X + y_M\, \boldsymbol{i}_Y$ and $\boldsymbol{\Lambda}_{\psi_L} = \boldsymbol{\Lambda}_\psi(\psi = \psi_L)$.

In other words, X_M, Y_M are the coordinates of the generic point M by respect to the global reference system, while x_M, y_M are the coordinate of the same point by respect to the mobile frame $\boldsymbol{e}_x(\psi_L), \boldsymbol{e}_y(\psi_L)$, having its origin at the end of the flexure-hinge.
The coordinates of the centre of instantaneous rotation (c.i.r.) X_C, Y_C (still unknown) of the mobile rigid body expressed in the global reference system, by definition, do not change for an infinitesimal motion:

$$d\boldsymbol{r}_C = 0 = d\boldsymbol{r}_L + \mathrm{d}\boldsymbol{r}_{CL} \tag{53}$$

The coordinates x_C, y_C of the c.i.r., expressed by respect to the mobile frame, do not modify during the infinitesimal motion due to the rigidity of the mobile rigid body. The only changeable terms are X_L, Y_L and $\boldsymbol{e}_x(\psi_L), \boldsymbol{e}_y(\psi_L)$, all functions of the final angle ψ_L (eq.s(2,47,48)). Hence:

$$\frac{d\boldsymbol{r}_C}{d\psi_L} = 0 = \frac{d\boldsymbol{r}_L}{d\psi_L} + \frac{d\boldsymbol{\Lambda}_{\psi_L}}{d\psi_L} \cdot \boldsymbol{x}_{CL} \;\Rightarrow\; \boldsymbol{x}_{CL} = -\left(\frac{d\boldsymbol{\Lambda}_{\psi_L}}{d\psi_L}\right)^T \frac{d\boldsymbol{r}_L}{d\psi_L} \tag{54}$$

Or, in components:

$$x_C(\psi_L) = \frac{dX_L}{d\psi_L} \sin\psi_L - \frac{dY_L}{d\psi_L} \cos\psi_L \tag{55}$$

$$y_C(\psi_L) = \frac{dX_L}{d\psi_L} \cos\psi_L + \frac{dY_L}{d\psi_L} \sin\psi_L \tag{56}$$

Eq.s(55,56) are the Cartesian equations of the mobile polode, namely the position of the c.i.r. by respect the mobile frame. Using eq.s(49,52,54), the equation of the fixed polode are given:

$$\boldsymbol{r}_C = \boldsymbol{r}_L - \boldsymbol{\Lambda}_{\psi_L} \cdot \left(\frac{d\boldsymbol{\Lambda}_{\psi_L}}{d\psi_L}\right)^T \frac{d\boldsymbol{r}_L}{d\psi_L} \tag{57}$$

Eq.(57) in components turn out:

$$X_C(\psi_L) = X_L - \frac{dY_L}{d\psi_L} \tag{58}$$

$$Y_C(\psi_L) = Y_L + \frac{dX_L}{d\psi_L} \tag{59}$$

The eq.s(55,56,58,59) are generally valid. In what follows, they are made explicit taking into account the case examined in §2.1. in which the flexure-hinge is loaded by different types of loads F_X^P, F_Y^P, M_Z^P; this scenario can be analytically explained using eq.s(47,48). Although eq.s(47,48) are valid only for flexure-hinges with constant section, all results obtained through the use of eq.s(47,48) may be extended to notched flexure hinges if an equivalent length of the main deformable part (with constant section) is estimated [63].
Differentiating eq.s(47,48) computed in $\psi = \psi_L$ by respect to ψ_L, considering that the terms c, F_X, F_Y are function of ψ_L, and Leibniz integration rule (differentiation under the integral sign) is used, it results:

$$\frac{dX_L}{d\psi_L} = \frac{sign(\psi_L')\cos\psi_L}{\left(\vartheta' + \frac{M_Z^L}{EI}\right)} - \int_{\psi_0}^{\psi_L} sign(\psi') \frac{df(\psi)}{d\psi_L} \frac{\cos\psi}{f(\psi)^2} d\psi \tag{60}$$

$$\frac{dY_L}{d\psi_L} = \frac{sign(\psi_L')\sin\psi_L}{\left(\vartheta' + \frac{M_Z^L}{EI}\right)} - \int_{\psi_0}^{\psi_L} sign(\psi') \frac{df(\psi)}{d\psi_L} \frac{\sin\psi}{f(\psi)^2} d\psi \tag{61}$$

where, using eq.s(30,31,B1,B2) for the derivatives of F_X, F_Y:

$$\frac{df(\psi)}{d\psi_L} = \frac{1}{EI\, f(\psi)}\left[\frac{dc}{d\psi_L} - \frac{dF_X^P}{d\psi_L}\cos\psi - \frac{dF_Y^P}{d\psi_L}\sin\psi\right] \tag{62}$$

differentiating eq.(38) using eq.(32):

$$\frac{dc}{d\psi_L} = \frac{dF_X^P}{d\psi_L}\cos\psi_L - F_X^P \sin\psi_L + \frac{dF_Y^P}{d\psi_L}\sin\psi_L + F_Y^P\cos\psi_L + \left(\vartheta' + \frac{M_Z^L}{EI}\right)\frac{dM_Z^L}{d\psi_L} \tag{63}$$

in which M_Z^L is reported in eq.(32), and its derivative is:

$$\frac{dM_Z^L}{d\psi_L} = \frac{dM_Z^P}{d\psi_L} + \left[\left(\frac{dF_Y^P}{d\psi_L} - F_X^P\right)x_P + \left(\frac{dF_X^P}{d\psi_L} - F_Y^P\right)y_P\right]\cos\psi_L + \tag{64}$$

$$-\left[\left(\frac{dF_X^P}{d\psi_L} + F_Y^P\right)x_P + \left(\frac{dF_Y^P}{d\psi_L} + F_X^P\right)y_P\right]\sin\psi_L$$

A dimensionless parameter $\tau \in [\tau_0, \tau_1]$ can be introduced to "chronologically" evaluate the trend of the loading-path. In other words, the parameter τ acts as an ordering variable, to identify the configuration change as a function of it. Therefore, the applied loads become a function of it $F_X^P(\tau), F_Y^P(\tau), F_X^P(\tau)$, where the loads applied at the initial and final configurations are $F_X^P(\tau_0), F_Y^P(\tau_0), M_Z^P(\tau_0)$ and $F_X^P(\tau_1), F_Y^P(\tau_1), M_Z^P(\tau_1)$ respectively (Figure 5).

As a consequence, the final angle $\psi_L(\tau)$ become a function of the parameter τ, and the derivatives that appear in eq.s(62-64) becomes:

$$\frac{dF_X^P}{d\psi_L} = \frac{\dot{F}_X^P}{\dot{\psi}_L} \quad ; \quad \frac{dF_Y^P}{d\psi_L} = \frac{\dot{F}_Y^P}{\dot{\psi}_L} \quad ; \quad \frac{dM_Z^P}{d\psi_L} = \frac{\dot{M}_Z^P}{\dot{\psi}_L} \tag{65}$$

where the notation $(\dot{\ })$ indicates the derivatives by respect the parameter τ.

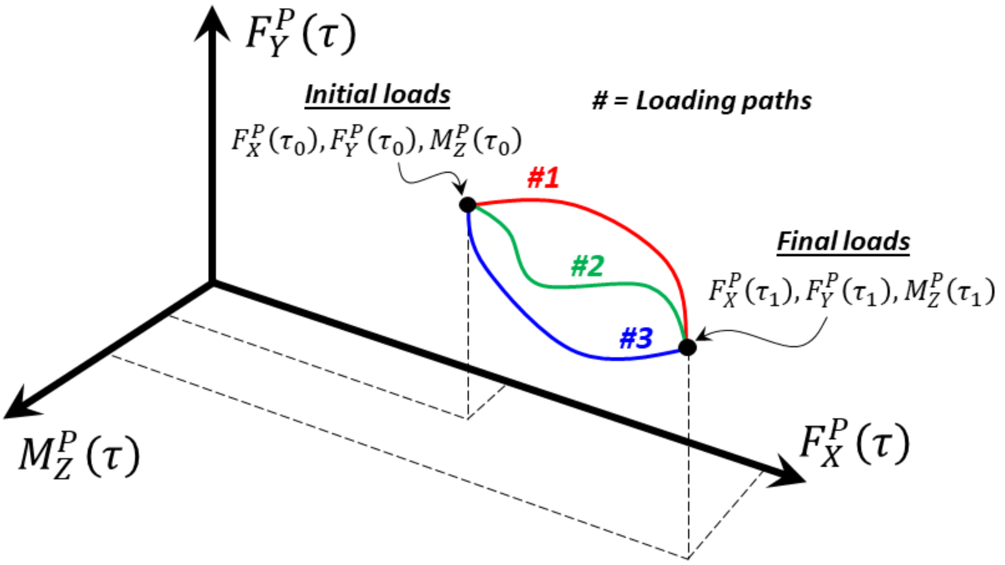

Figure 5. Generic loading paths

To recap, for one d.o.f. rigid mechanisms, ψ_L is a function of time t and the relationship between them would result unique; this implies that the polodes are instantaneous geometric invariants. For a compliant mechanism, instead, ψ_L is a function of the applied loads' intensity but also of the loading-histories and loading-rates. In other words, the polodes are not conservative; if two different loading-paths are applied (e.g. two different motion time-laws to obtain two different dynamic loads), the c.i.r. locations (i.e. fixed and mobile polodes) differ. Therefore, the polodes are not instantaneous geometric invariants, and for compliant mechanisms instantaneous-invariants that are independent of the motion time-law cannot be assessed.

There is only one situation where, for static loading, the polodes are conservative (i.e. are not loading-path dependents); this occurs when the flexure-hinge are loaded by only a concentrated moment. For this case, a fully analytical solution of the fixed and mobile polodes is provided in Appendix D.

Another important instantaneous invariant that is worth to define analytically is the first Bresse's circle (or inflection circle) [59,62,64,65]. It is the locus of points that instantaneously translate (i.e. have zero normal acceleration). The curvature of a generic point M of the mobile rigid body (Figure 4) is:

$$k_M = \frac{\frac{dX_M}{d\psi_L}\frac{d^2Y_M}{d{\psi_L}^2} - \frac{d^2X_M}{d{\psi_L}^2}\frac{dY_M}{d\psi_L}}{\left[\left(\frac{dX_M}{d\psi_L}\right)^2 + \left(\frac{dY_M}{d\psi_L}\right)^2\right]^{\frac{3}{2}}} \tag{66}$$

To find the locus of points X_{in}, Y_{in} which have zero normal acceleration (i.e. an instantaneous inflection in their trajectory), hence zero curvature of their trajectory, it is sufficient to set to zero the eq.(66):

$$\frac{dX_{in}}{d\psi_L}\frac{d^2Y_{in}}{d{\psi_L}^2} - \frac{d^2X_{in}}{d{\psi_L}^2}\frac{dY_{in}}{d\psi_L} = 0 \tag{67}$$

Using eq.(49), one obtains:

$$\frac{dX_{in}}{d\psi_L} = \frac{dX_L}{d\psi_L} - x_{in}\,\sin\psi_L - y_{in}\,\cos\psi_L \tag{68}$$

$$\frac{d^2X_{in}}{d{\psi_L}^2} = \frac{d^2X_L}{d{\psi_L}^2} - x_{in}\,\cos\psi_L + y_{in}\,\sin\psi_L \tag{69}$$

$$\frac{dY_{in}}{d\psi_L} = \frac{dY_L}{d\psi_L} + x_{in}\,\cos\psi_L - y_{in}\,\sin\psi_L \tag{70}$$

$$\frac{d^2Y_{in}}{d{\psi_L}^2} = \frac{d^2Y_L}{d{\psi_L}^2} - x_{in}\,\sin\psi_L - y_{in}\,\cos\psi_L \tag{71}$$

Applying eq.s(68-71) the eq.(67) turns out:

$$ {x_{in}}^2 + {y_{in}}^2 + a\,x_{in} + b\,y_{in} + c = 0 \tag{72}$$

where:

$$a = \left(\frac{dY_L}{d\psi_L} - \frac{d^2X_L}{d{\psi_L}^2}\right)\cos\psi_L - \left(\frac{dX_L}{d\psi_L} + \frac{d^2Y_L}{d{\psi_L}^2}\right)\sin\psi_L \tag{73}$$

$$b = \left(\frac{d^2X_L}{d{\psi_L}^2} - \frac{dY_L}{d\psi_L}\right)\sin\psi_L - \left(\frac{d^2Y_L}{d{\psi_L}^2} + \frac{dX_L}{d\psi_L}\right)\cos\psi_L \tag{74}$$

$$c = \frac{dX_L}{d\psi_L}\frac{d^2Y_L}{d{\psi_L}^2} - \frac{d^2X_L}{d{\psi_L}^2}\frac{dY_L}{d\psi_L} \tag{75}$$

Eq.(72) is a circumference. Therefore, the parametric equations of the inflection circle by respect to the mobile frame are:

$$x_{in} = c_x + R\cos u \tag{76}$$

$$y_{in} = c_y + R\sin u \tag{77}$$

where $u \in [0,2\pi]$ is the parameter, $\boldsymbol{C} = c_x\,\boldsymbol{i}_X + c_y\,\boldsymbol{i}_Y = -\frac{1}{2}[a\,\boldsymbol{i}_X + b\,\boldsymbol{i}_Y]$, $R = \frac{1}{2}\sqrt{a^2 + b^2 - 4c}$ are the centre and radius of the inflection circle (74,75). The parametric equations of the inflection circle by respect the fixed frame are (eq.(49)):

$$X_{in} = X_L + x_{in}\,\cos\psi_L - y_{in}\,\sin\psi_L \tag{78}$$

$$Y_{in} = Y_L + x_{in}\,\sin\psi_L + y_{in}\,\cos\psi_L \tag{79}$$

The eq.s(76-79) of the inflection circle are analytically defined if the second derivative of X_L, Y_L is made explicit (prime derivative is defined by eq.s(60,61)). Therefore, differentiating eq.s(60,61) one obtains:

$$\begin{aligned}\frac{d^2X_L}{d{\psi_L}^2} = {} & \frac{sign(\psi_L')\ \cos\psi_L}{EI\left(\vartheta' + \frac{M_Z^L}{EI}\right)^3}\left[F_Y^P\cos\psi_L - F_X^P\sin\psi_L + \left(\vartheta' + \frac{M_Z^L}{EI}\right)\frac{dM_Z^L}{d\psi_L}\right] + \\ & -\frac{sign(\psi_L')\sin\psi_L}{\left(\vartheta' + \frac{M_Z^L}{EI}\right)} - \frac{sign(\psi_L')\cos\psi_L}{EI\left(\vartheta' + \frac{M_Z^L}{EI}\right)^2}\,\frac{dM_Z^L}{d\psi_L} + \\ & -\int_{\psi_0}^{\psi_L}\frac{sign(\psi')\ \cos\psi}{f(\psi)^2}\left[\frac{d^2f(\psi)}{d{\psi_L}^2} - \frac{2}{f(\psi)}\left(\frac{df(\psi)}{d\psi_L}\right)^2\right]d\psi\end{aligned} \tag{80}$$

$$\begin{aligned}\frac{d^2Y_L}{d{\psi_L}^2} = {} & \frac{sign(\psi_L')\ \sin\psi_L}{EI\left(\vartheta' + \frac{M_Z^L}{EI}\right)^3}\left[F_Y^P\cos\psi_L - F_X^P\sin\psi_L + \left(\vartheta' + \frac{M_Z^L}{EI}\right)\frac{dM_Z^L}{d\psi_L}\right] + \\ & -\frac{sign(\psi_L')\cos\psi_L}{\left(\vartheta' + \frac{M_Z^L}{EI}\right)} - \frac{sign(\psi_L')\sin\psi_L}{EI\left(\vartheta' + \frac{M_Z^L}{EI}\right)^2}\,\frac{dM_Z^L}{d\psi_L} + \\ & -\int_{\psi_0}^{\psi_L}\frac{sign(\psi')\ \sin\psi}{f(\psi)^2}\left[\frac{d^2f(\psi)}{d{\psi_L}^2} - \frac{2}{f(\psi)}\left(\frac{df(\psi)}{d\psi_L}\right)^2\right]d\psi\end{aligned} \tag{81}$$

where:

$$\begin{aligned}\frac{d^2f(\psi)}{d{\psi_L}^2} = {} & \frac{1}{EI\,f(\psi)}\left[\frac{d^2c}{d{\psi_L}^2} + \left(\frac{dF_Y^P}{d\psi_L} - \frac{d^2F_X^P}{d{\psi_L}^2}\right)\cos\psi + \left(\frac{dF_X^P}{d\psi_L} - \frac{d^2F_Y^P}{d{\psi_L}^2}\right)\sin\psi + \right] \\ & + \frac{1}{f(\psi)}\left(\frac{df(\psi)}{d\psi_L}\right)^2\end{aligned} \tag{82}$$

$$\begin{aligned}\frac{d^2c}{d{\psi_L}^2} = {} & \left(\frac{d^2F_X^P}{d{\psi_L}^2} - F_X^P + \frac{dF_Y^P}{d\psi_L}\right)\cos\psi_L + \left(\frac{d^2F_Y^P}{d{\psi_L}^2} - \frac{dF_X^P}{d\psi_L} - F_Y^P\right)\sin\psi_L + \\ & + \left(\frac{1}{EI}\frac{dM_Z^L}{d\psi_L}\right)^2 + \left(\vartheta' + \frac{M_Z^L}{EI}\right)\frac{d^2M_Z^L}{d{\psi_L}^2}\end{aligned} \tag{83}$$

$$\frac{d^2M_Z^L}{d{\psi_L}^2} = \frac{d^2M_Z^P}{d{\psi_L}^2} + \left[\left(\frac{d^2F_Y^P}{d{\psi_L}^2} - 2\frac{dF_X^P}{d\psi_L} - F_Y^P\right)x_P + \left(\frac{d^2F_X^P}{d{\psi_L}^2} - 2\frac{dF_Y^P}{d\psi_L} - F_X^P\right)y_P\right]\cos\psi_L \tag{84}$$

$$-\left[\left(2\frac{dF_Y^P}{d\psi_L}-F_X^P+\frac{d^2F_X^P}{d\psi_L{}^2}\right)x_P+\left(2\frac{dF_X^P}{d\psi_L}-F_Y^P+\frac{d^2F_Y^P}{d\psi_L{}^2}\right)y_P\right]\sin\psi_L$$

In which:

$$\frac{d^2F_X^P}{d\psi_L{}^2}=\ddot{F}_X^P-\frac{\dot{F}_X^P}{\dot{\psi}_L}\ddot{\psi}_L \quad ; \quad \frac{d^2F_Y^P}{d\psi_L{}^2}=\ddot{F}_Y^P-\frac{\dot{F}_Y^P}{\dot{\psi}_L}\ddot{\psi}_L \quad ; \quad \frac{d^2M_Z^P}{d\psi_L{}^2}=\ddot{M}_Z^P-\frac{\dot{M}_Z^P}{\dot{\psi}_L}\ddot{\psi}_L \tag{85}$$

For the case in which only a concentrated moment is applied, a fully analytical solution of the inflection circle is reported Appendix D. Following the flow of what above done, it is possible to find the analytical description of many other geometric loci important for the kinematic synthesis: the second Bresse's circle, the centre of accelerations, the cubic of stationary curvature, the Burmester points, etc.

4. Numerical examples and experimental evidence

In this section some numerical applications of the results obtained in §2 and §3 are shown. The analytical formulation given by eq.s (46-48) is used. If length, bending stiffness and loads are given, the only unknown is the angle ψ_L. The latter needs to be obtained using an attempt method on eq.(46). A fast method to address this issue is the bisection algorithm [31,33,45], which requires an interval search $\psi_L \in [\psi_{L1}, \psi_{L2}]$ (which can be chosen very wide, e.g. $(0,2\pi)$ to satisfy any load and configuration conditions). The error tolerance of the end angle is set to 10^{-8} in the following examples.

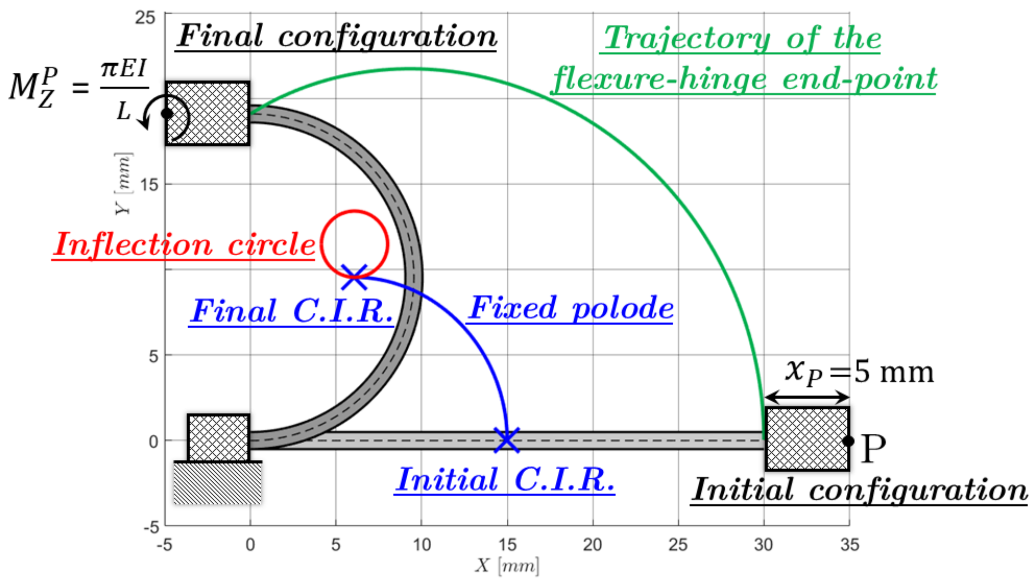

Figure 6. Flexure-hinge loaded by a concentrated moment applied to the mobile rigid body

The kinematic of a flexure-hinge connecting to two rigid bodies, constrained and mobile, is examined. The material of the flexure-hinge is ABS with $E = 2.3\ GPa$, the length is $L = 30\ mm$, and the constant section is rectangular, $1\ mm$ thick and $3\ mm$ wide. The load is applied on the mobile rigid body at $x_P = 5\ mm$.

The first case (Figure 6) concerns a straight flexure-hinge, where a pure moment acts on the mobile rigid body. This situation gives a fully analytical solution reported in Appendix D. The applied moment is set equal to $M_Z^P = \pi EI/L$, such as to obtain a final angle $\psi_L = \pi$. Figure 6 shows the trajectory of the end-point and of the c.i.r. (i.e. the fixed polode), and the inflection circle computed in the final configuration. This is a special case, inasmuch the presence of only one type of load guarantees that the polode is conservative, i.e. loading-path undependent. It is possible to observe that the initial position of the c.i.r.

coincides with the centre of the flexure-hinge, but it moves away during the configuration change, being located more and more out of the flexure-hinge axis and closer to the fixed body. For this reason, the pseudo-rigid body approach due to the Howell's simplest version [2], which involves a single lumped hinge in the middle of the flexure-hinge, causes a significant error in the predicted motion [40].

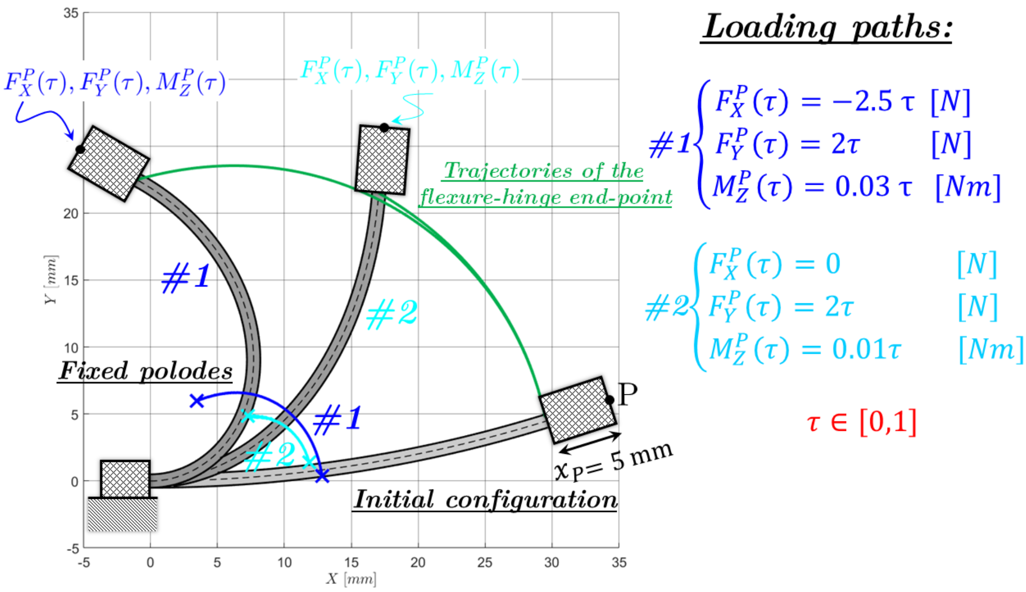

Figure 7. Flexure-hinge loaded by two different loading-paths

A less trivial example is shown in Figure 7. In this case, an initially curved flexure-hinge ($\vartheta' = 10\,m^{-1}$) is connected to a rigid body loaded with both forces and a moment. The two loading paths (detailed in Figure 7) have a linear trend but two different final loads. As could be expected, for two different final loads the two fixed polodes differ, and therefore all the instantaneous invariants (being them dependent on the location of the c.i.r.).

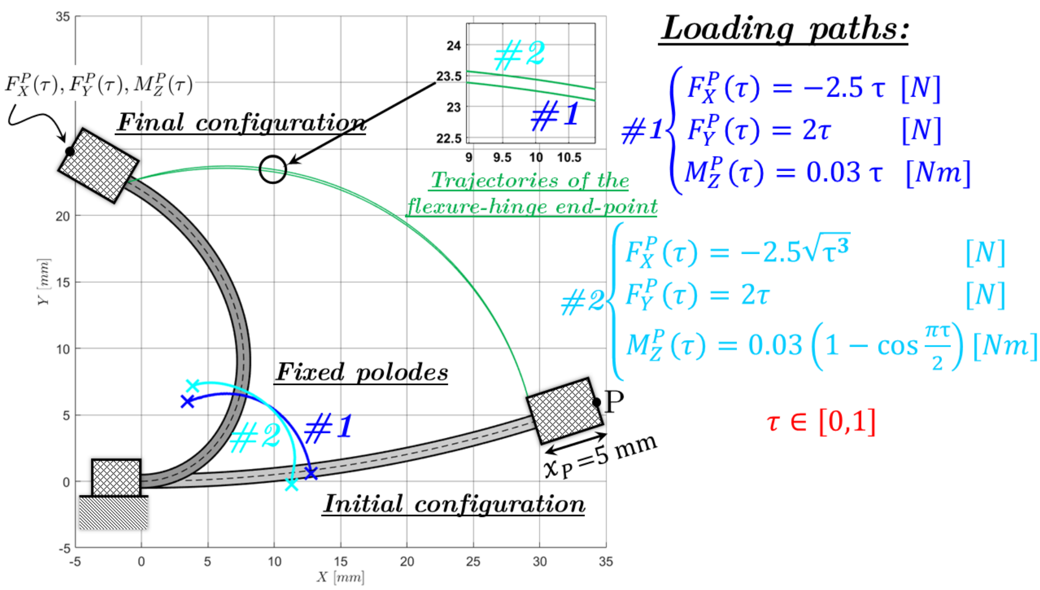

Figure 8. Flexure-hinge loaded by two loading-paths with the same final loads but different rate-trends

The case in Figure 8 examines the influence of the loading-trend on the c.i.r. locations, keeping the same final loads. The first loading-path is the same as above, while the second achieves the same final loads, but they grow in a nonlinear way.
The two fixed polodes differ, as is evident in Figure 8. Note that the initial positions of the c.i.r. do not coincide either.
This result is less intuitive than the previous one, but it proves that, generally, instantaneous invariants are not conservative for compliant mechanisms.
Therefore, it is not possible to foresee the motion and their features (i.e. instantaneous invariants) of whatever flexible mechanism if the dynamic knowledge of all acting loads is unknown. In the above presented examples, indeed, the c.i.r. locations differ remarkably. In other words, one should be very careful to address the kinematic synthesis of compliant mechanisms using the same method used for rigid ones connected through kinematic pairs.

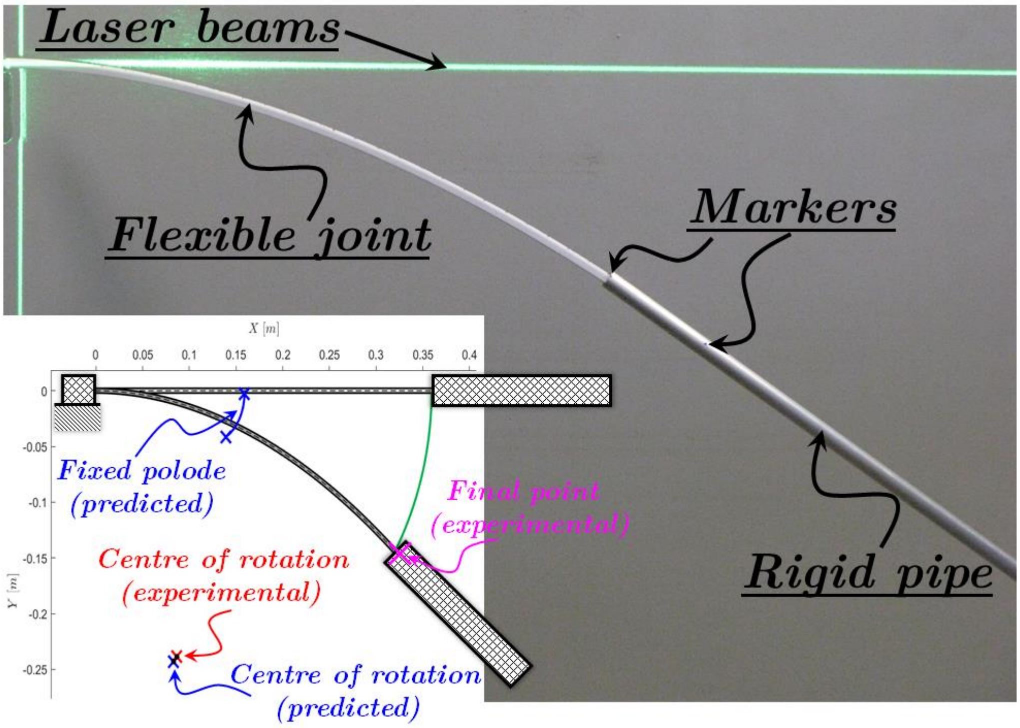

Figure 9. Experimental setup

Some experiments have been conducted on flexible PVC beam, constrained with two almost rigid pipes at the ends; one is fixed, and the other, free, is subjected to gravity, as shown in Figure 9. The bending stiffness of the flexible beam has been estimated through material testing and section measurement. The extrapolation of experimental data is conducted through a digital image analysis by the alinement of the instruments throgh laser beams. The same experimental measurements are used to perform the method introduced in this paper. The comparisons between experimental evidence and numerical prediction compare the overall (i.e. between the initial and final configuration) centre of rotation, as shown in Figure 9 (first case of Table 1). The two centres of rotation are close, demonstrating that the method allows correctly following considerable displacements. It is interesting to evidence that the trajectory of the c.i.r. (i.e. the fixed polode) during the motion are not a-priori predictable only by knowledge of the initial and final configurations, but it is mandatory to perform a reliable kinematic analysis. In Table 1 four cases are examined according to the length of the flexible-joint, where the experimental and predicted coordinates of the centre of rotation and final angles are reported. All the results show good agreement with small or relevant displacements, but the error increases inversely proportional to the length, probably due to lower precision of data acquisition if compared with the total displacement.

Table 1. Experimental and predicted position of rotation's centre and final end-angle for four lengths of flexible-joint.

Flexible-joint lenghts [mm]	Experimental centre of rotation [mm]	Predicted centre of rotation [mm]	Experimental final angle [deg]	Predicted final angle [deg]
360	(87.3, -238.6)	(83.7, -242.9)	41.6	42.7
270	(85.2, -169.4)	(85.3, -168.2)	33.0	32.6
180	(70.7, -100.1)	(71.4, -97.4)	22.2	21.5
90	(40.3, -47.1)	(41.5, -38.9)	12.47	10.16

5. Conclusions

The paper investigates the elasto-kinematics and the kinematic-features of motion (i.e. instantaneous invariants) of compliant mechanisms based on flexure-hinges. A comprehensive deduction of the differential equation that governs flexure-hinge's nonlinear geometric behaviour is presented. These equations are analytically addressed, assuming that extensional and shear strains are neglected, the section and the initial curvature are constant, and the distributed loads are null. The analytical solution provides remarkable computationally advantages compared to numerical methods (e.g. Runge-Kutta); it allows managing a single point of interest (e.g. the extreme of the flexure-hinge), avoiding a full-length integration. This feature is crucial to deduce the analytical expressions of instantaneous invariants that require the derivatives of the end-point of the flexure-hinge. Two instantaneous invariants are investigated, the centre of instantaneous rotation (c.i.r.) and the inflection circle (first Bresse's circle). The main obtained result is that the c.i.r. locations (i.e. fixed polode) are not conservative, i.e. they depend on the loading-path. Therefore, all the other instantaneous invariants are not conservative; as a consequence, the notion of instantaneous geometric invariants (i.e. undependent on the motion time-law) decays. These results are numerically verified in some examples, and a simple experimental validation has been conducted by optical means with the aim to verify that the step-by-step analysis drives to the final configuration experienced.
The obtained equation, although given for flexure-hinge with constant section, may be extended to notched flexure hinges observing that the main deformation is due to the central part with constant section. Furthermore, the achieved results could open a way to define the Jacobian constraint matrix (used in multibody codes) of flexure-hinges, where it should appear not only as a function of the geometry and material properties but also of the applied loads.

Appendix A – Proof of the skewness of the Curvature Tensor

The change-of-basis $\boldsymbol{\Lambda}$ is an orthogonal tensor:

$$\boldsymbol{\Lambda}(\boldsymbol{\Lambda})^T = \boldsymbol{I} \tag{A1}$$

Applying the derivative by respect to s of the eq.(A1), it turns out:

$$\frac{\partial \boldsymbol{\Lambda}}{\partial s}(\boldsymbol{\Lambda})^T = -\boldsymbol{\Lambda}\frac{\partial (\boldsymbol{\Lambda})^T}{\partial s} = -\left[\frac{\partial \boldsymbol{\Lambda}}{\partial s}(\boldsymbol{\Lambda})^T\right]^T \tag{A2}$$

That is the definition of a skew-symmetric tensor. Therefore, the curvature tensors in eq.(7,8) are skew-symmetric.

Appendix B – Other relations regarding the equilibrium

The forces and moment $\boldsymbol{F}(s), \boldsymbol{M}(s)$ applied at the generic curvilinear abscissa s can also be expressed as functions of the applied loads $\boldsymbol{F}_L, \boldsymbol{M}_L$ at $s = L$, as well as the distributed loads:

$$F_X(s) = F_X^L + \int_s^L q_X(\tilde{s})\, d\tilde{s} \tag{B1}$$

$$F_Y(s) = F_Y^L + \int_s^L q_Y(\tilde{s})\, d\tilde{s} \tag{B2}$$

$$M_Z(s) = M_Z^L - (Y_L - Y)F_X^L + (x_L - x)F_Y^L + \tag{B3}$$

$$+ \int_s^L \left[-\left(\tilde{Y} - Y\right) q_X(\tilde{s}) - \left(\tilde{X} - X\right) q_Y(\tilde{s}) + m_Z(\tilde{s}) \right] d\tilde{s}$$

where $X_L = X(s = L)$, $Y_L = Y(s = L)$ are the coordinates of the point in $s = L$.
By applying the moment equilibrium with the pole at $s = 0$, the components of $\boldsymbol{F}_0, \boldsymbol{M}_0$ can be expressed as function of $\boldsymbol{F}_L, \boldsymbol{M}_L$:

$$F_X^0 = -F_X^L - \int_0^L q_X(s)\, ds \tag{B4}$$

$$F_Y^0 = -F_Y^L - \int_0^L q_Y(s)\, ds \tag{B5}$$

$$M_Z^0 = -M_Z^L + Y_L F_X^L - X_L F_Y^L + \tag{B6}$$

$$+ \int_0^L \left[Y\, q_X(s) - X\, q_Y(s) - m_Z(s) \right] ds$$

On the contrary, by applying the moment equilibrium with the pole at $s = L$, the components of $\boldsymbol{F}_L, \boldsymbol{M}_L$ can be expressed as function of $\boldsymbol{F}_0, \boldsymbol{M}_0$:

$$F_X^L = -F_X^0 - \int_0^L q_X(s)\, ds \tag{B7}$$

$$F_Y^L = -F_Y^0 - \int_0^L q_Y(s)\, ds \tag{B8}$$

$$M_Z^L = -M_Z^0 - Y_L F_X^0 + X_L F_Y^0 + \tag{B9}$$

$$+ \int_0^L \left[-(Y_L - Y) q_X(s) - (X_L - X) q_Y(s) - m_Z(s) \right] ds$$

Appendix C – A useful trick to avoid the singularities of some integrals

In the presence of an inflection point, the denominator of the eq.s(42-44) becomes null for $\psi(s) = \psi_{in}$. If an internal inflection point occurs at $\psi(s) = \psi_i$ the integral of eq.(42), using eq.(41) also, can be separated into two contributes:

$$L = \int_{\psi_0}^{\psi_{in}} \frac{sign(\psi')}{f(\psi)} d\psi + \int_{\psi_{in}}^{\psi_L} \frac{sign(\psi')}{f(\psi)} d\psi \tag{C1}$$

The previous integrand function becomes singular for ψ_i. Therefore, to overcome this problem [66], we introduce a very small positive quantity $\epsilon \ll 1$ (numerically $\epsilon \cong 10^{-4}$ can be sufficient) such that:

$$L = sign(\psi_0')\left[\int_{\psi_0}^{\psi_i-\epsilon} \frac{d\psi}{f(\psi)} + \int_{\psi_{in}-\epsilon}^{\psi_{in}} \frac{d\psi}{f(\psi)}\right] + sign(\psi_L')\left[\int_{\psi_{in}+\epsilon}^{\psi_L} \frac{d\psi}{f(\psi)} + \int_{\psi_{in}}^{\psi_{in}+\epsilon} \frac{d\psi}{f(\psi)}\right] \quad \text{(C2)}$$

The two integrals with extremes of integration $[\psi_{in}-\epsilon,\ \psi_{in}]$ and $[\psi_{in},\ \psi_{in}+\epsilon]$, by virtue of the smallness of ϵ can be linearized (and then integrated) using the change of variables $\psi = \psi_{in} - \omega$, that implies $\omega \in [0, \epsilon]$, obtaining:

$$f(\psi) = f(\psi_{in} - \omega) \cong \quad \text{(C3)}$$

$$\cong \sqrt{\frac{2}{EI}[c - F_X(\cos\psi_{in} + \omega\sin\psi_{in}) - F_Y(\sin\psi_{in} - \omega\cos\psi_{in})]}$$

Hence:

$$I_1(\epsilon) = \int_{\psi_{in}-\epsilon}^{\psi_{in}} \frac{d\psi}{f(\psi)} = \int_0^{\epsilon} \frac{d\omega}{f(\psi_{in}-\omega)} = \sqrt{2EI}\,\frac{\sqrt{\tilde{A}+\epsilon\tilde{B}} - \sqrt{\tilde{A}}}{\tilde{B}} \quad \text{(C4)}$$

$$I_2(\epsilon) = \int_{\psi_{in}}^{\psi_{in}+\epsilon} \frac{d\psi}{f(\psi)} = \int_{-\epsilon}^{0} \frac{d\omega}{f(\psi_{in}-\omega)} = \sqrt{2EI}\,\frac{\sqrt{\tilde{A}} - \sqrt{\tilde{A}-\epsilon\tilde{B}}}{\tilde{B}} \quad \text{(C5)}$$

where:

$$\tilde{A} = c - F_X\cos\psi_{in} - F_Y\sin\psi_{in} \quad \text{(C6)}$$

$$\tilde{B} = F_Y\cos\psi_{in} - F_X\sin\psi_{in} \quad \text{(C7)}$$

Therefore, the integral of eq.(43) (or eq.(C1)) in the presence of an inflection point turn out as:

$$L = sign(\psi_0')\left[\int_{\psi_0}^{\psi_{in}-\epsilon} \frac{d\psi}{f(\psi)} + I_1\right] + sign(\psi_L')\left[\int_{\psi_{in}+\epsilon}^{\psi_L} \frac{d\psi}{f(\psi)} + I_2\right] \quad \text{(C8)}$$

and the singularity no longer appears.

The same trick can be applied to the integrals in eq.(44,45), obtaining:

$$X(\psi) = X_0 + sign(\psi_0')\left[\int_{\psi_0}^{\psi_{in}-\epsilon} \frac{\cos\tilde{\psi}}{f(\tilde{\psi})} d\tilde{\psi} + I_3\right] + \quad \text{(C9)}$$

$$+ sign(\psi_L')\left[\int_{\psi_{in}+\epsilon}^{\psi} \frac{\cos\tilde{\psi}}{f(\tilde{\psi})} d\tilde{\psi} + I_4\right]$$

$$Y(\psi) = y_0 + sign(\psi_0')\left[\int_{\psi_0}^{\psi_{in}-\epsilon} \frac{\sin\tilde{\psi}}{f(\tilde{\psi})} d\tilde{\psi} + I_5\right] + \quad \text{(C10)}$$

$$+ sign(\psi_L')\left[\int_{\psi_{in}+\epsilon}^{\psi} \frac{\sin\tilde{\psi}}{f(\tilde{\psi})} d\tilde{\psi} + I_6\right]$$

where:

$$I_3(\epsilon) = \frac{I_1(\epsilon)\cos\psi_{in}}{sign(\psi_L')} + \frac{2\sin\psi_{in}}{3\tilde{B}^2}\left[\left(\epsilon\tilde{B} - 2\tilde{A}\right)\sqrt{\tilde{A} + \epsilon\tilde{B}} + 2\tilde{A}\sqrt{\tilde{A}}\right] \tag{C11}$$

$$I_4(\epsilon) = \frac{I_2(\epsilon)\cos\psi_{in}}{sign(\psi_L')} + \frac{2\sin\psi_{in}}{3\tilde{B}^2}\left[\left(\epsilon\tilde{B} + 2\tilde{A}\right)\sqrt{\tilde{A} - \epsilon\tilde{B}} - 2\tilde{A}\sqrt{\tilde{A}}\right] \tag{C12}$$

$$I_5(\epsilon) = \frac{I_1(\epsilon)\sin\psi_{in}}{sign(\psi_L')} + \frac{2\cos\psi_{in}}{3\tilde{B}^2}\left[\left(\epsilon\tilde{B} - 2\tilde{A}\right)\sqrt{\tilde{A} + \epsilon\tilde{B}} + 2\tilde{A}\sqrt{\tilde{A}}\right] \tag{C13}$$

$$I_6(\epsilon) = \frac{I_2(\epsilon)\sin\psi_{in}}{sign(\psi_L')} + \frac{2\cos\psi_{in}}{3\tilde{B}^2}\left[\left(\epsilon\tilde{B} + 2\tilde{A}\right)\sqrt{\tilde{A} - \epsilon\tilde{B}} - 2\tilde{A}\sqrt{\tilde{A}}\right] \tag{C14}$$

It is worth pointing out that the eq.s(C2,C9,C10) hold even if an inflection point happens at one end (e.g. a cantilever beam loaded by a concentrates force at the end)), simply considering that $\psi_{in} = \psi_0$ or $\psi_{in} = \psi_L$.

Appendix D – Fully Analytical solution of polodes (fixed and mobile) and inflection circle for a flexure-hinge loaded by a concentrated moment

Taking into account the assumptions of §2.1, the deformed configuration of a flexure-hinge loaded only by a concentrated moment M_Z^P is represented by the following parametric equations [53]:

$$\psi(s) = \psi_0 + \left(\vartheta' + \frac{M_Z^P}{EI}\right)s \tag{D1}$$

$$X(s) = X_0 + \frac{\sin\left[\left(\vartheta' + \frac{M_Z^P}{EI}\right)s\right]}{\left(\vartheta' + \frac{M_Z^P}{EI}\right)} \tag{D2}$$

$$Y(s) = Y_0 + \frac{1 - \cos\left[\left(\vartheta' + \frac{M_Z^P}{EI}\right)s\right]}{\left(\vartheta' + \frac{M_Z^P}{EI}\right)} \tag{D3}$$

From the latter equations, the terms $X_L, Y_L, \frac{dX_L}{d\psi_L}, \frac{dY_L}{d\psi_L}, \frac{d^2X_L}{d\psi_L{}^2}, \frac{d^2Y_L}{d\psi_L{}^2}$ that forms the parametric equations of the fixed and mobile polodes in eq.s(55,56,58,59) and the inflection circle in eq.s(74-77) can be made explicit. Setting $\psi_0 = X_0 = Y_0 = 0$ for the sake of clarity, one obtains:

$$\psi_L = \left(\vartheta' + \frac{M_Z^P}{EI}\right)L \tag{D4}$$

$$X_L = \frac{L\ \sin\psi_L}{\psi_L} \tag{D5}$$

$$Y_L = \frac{L\ (1 - \cos\psi_L)}{\psi_L} \tag{D6}$$

$$\frac{dX_L}{d\psi_L} = \frac{L - X_L}{\psi_L} - Y_L \tag{D7}$$

$$\frac{dY_L}{d\psi_L} = X_L - \frac{Y_L}{\psi_L} \tag{D8}$$

$$\frac{d^2X_L}{d{\psi_L}^2} = \frac{X_L - L}{{\psi_L}^2} - \frac{dY_L}{d\psi_L} - \frac{1}{\psi_L}\frac{dX_L}{d\psi_L} \tag{D9}$$

$$\frac{d^2Y_L}{d{\psi_L}^2} = \frac{dX_L}{d\psi_L} - \frac{1}{\psi_L}\frac{dY_L}{d\psi_L} + \frac{Y_L}{{\psi_L}^2} \tag{D10}$$

References

1. Howell, L.L.; Magleby, S.P.; Olsen, B.M. Handbook of Compliant Mechanisms, *Wiley*, 2013, New York.
2. Howell, L.L. Compliant Mechanisms, *John Wiley and Sons*, 2001, Inc, USA.
3. Alejandro, A.E.; Fachinotti, V. D.; Pucheta, M.A. A review on design methods for compliant mechanisms. A Mecánica Computacional Vol XXIX, 2010, págs. 59-72, Dvorkin E., Goldschmit M., Storti M. (Eds.)
4. Shuib,S; Ridzwan, M.I.Z.; Kadarman, A.H. Methodology of compliant mechanisms and its current developments in applications: a review, Am. J. Appl. Sci., 2007, 4 (3), 160–167.
5. Jagtap, S.P.; Deshmukh, B.B.; Pardeshi, S. Applications of compliant mechanism in today's world – A review, *J. Phys.: Conf. Ser.*, 2021, 012013.
6. Wu, S.; Shao, Z.; Fu, H. A Substructure Condensed Approach for Kinetostatic Modeling of Compliant Mechanisms with Complex Topology. *Micromachines*, 2022, 13, 1734. https://doi.org/ 10.3390/mi13101734
7. Lin, S.;Wang, J.; Xiong,W.; Hu, Q.; Liu, H.; Wang, Q. Design and Modeling of a Curved Beam Compliant Mechanism with Six Degrees of Freedom. *Micromachines* 2022, 13, 208. https://doi.org/ 10.3390/mi13020208.
8. Liu, T.; Hao, G. Design of Deployable Structures by Using Bistable Compliant Mechanisms. *Micromachines* 2022, 13, 651. https://doi.org/10.3390/ mi13050651.
9. Xi, X.; Clancy, T.; Wu, X.; Sun, Y; Liu, X. A MEMS XY-stage integrating compliant mechanism for nanopositioning at sub-nanometer resolution, J. *Micromech. Microeng*., 2016, 26-025014.
10. Kota, S.; Joo, J.; Li, Z.; Rodgers, S.M.; Sniegowski, J. Design of Compliant Mechanisms: Applications to MEMS. *Analog Integrated Circuits and Signal Processing*, *Kluwer Academic Publishers*, 2001, 29, 7–15.
11. Parkinson, M.; Jensen, B.; Kurabayashi, K. Design of compliant force and displacement amplification micro-mechanisms, *Proceedings of DETC ASME*, 2001.
12. Kahr,M.; Steiner, H; Hortschitz, W.; Stifter, M.; Kainz, A; Keplinger, F. 3D-Printed MEMS Magnetometer Featuring Compliant Mechanism, *Proceedings*, 2018, 2(13), 784.
13. Iqbal, S; Lai, Y; Shakoor, R.I.; Raffi, M.; Bazaz, S.A. Design, analysis, and experimental investigation of micro-displacement amplification compliant mechanism for micro-transducers. *Rev. Sci. Instrum*., 2021, 92, 105007.
14. Ursi, P.; Rossi, A.; Botta, F.; Belfiore, N.P. Analytical Modeling of a New Compliant Microsystem for Atherectomy Operations. *Micromachines*, 2022, 13, 1094. https://doi.org/10.3390/ mi13071094
15. Botta, F.; Rossi, A.; Belfiore, N.P. A Cantilever-Based Piezoelectric MEMS for Arbitrary XY Path Generation. *Micromachines*, 2022, 13, 1514. https://doi.org/10.3390/ mi13091514.
16. Botta, F. A Piezoelectric MEMS Microgripper for Arbitrary XY Trajectory. *Micromachines*, 2022, 13, 1888. https://doi.org/10.3390/ mi13111888.
17. Botta, F.; Rossi, A.; Belfiore, N.P. A Feasibility Study of a Novel Piezo MEMS Tweezer for Soft Materials Characterization. *Appl. Sci.*, 2019, 9, 2277. doi:10.3390/app9112277
18. Di Giamberardino, P.; Bagolini, A; Bellutti, P.; Rudas, I.J.; Verotti, M.; Botta, F.; Belfiore, N.P. New MEMS Tweezers for the Viscoelastic Characterization of Soft Materials at the Microscale. *Micromachines*, 2018, 9, 15; doi:10.3390/mi9010015.
19. Laszczyk, K; Bargiel, S.; Gorecki, C.; Krezel, J.; Dziubana, P; Kujawinskab, M.; Callet, D.; Frankd, S. A two directional electrostatic comb-drive X–Y micro-stage for MOEMS applications. *Sensors and Actuators A: Physical*, 2010, A 163, 255–265.
20. Singh, J; Teo, J.H.S.; Xu, Y; Premachandran, C.S.; Chen, N.; Kotlanka, R.; Olivo, M. Sheppard, C.J.R. A two axes scanning SOI MEMS micromirror for endoscopic bioimaging, *J. Micromech. Microeng*., 2008, 18, 1–9.
21. Smith, S.T.; Chetwynd, D.G.; Bowen, D.K. Design and assessment of monolithic high precision translation mechanisms. *J. Phys. E Sci. Instrum*, 1987, 20, 977–983.
22. Linß, S.; Schorr, P.; Zentner, L. General design equations for the rotational stiffness, maximal angular deflection and rotational precision of various notch flexure hinges. *Mech. Sci.*, 2017, 8, 29–49.
23. Hou, W. Analysis of three nodes flexure hinge element in ultra-precision positioning stage. *Proceedings of the 7th International Conference on Biomedical Engineering and Informatics*, 2014, Dalian, China, 14–16 October 2014; pp. 527–533.
24. Melgarejo, M.; Darnieder, M; Linß, S.; Zentner, L.; Fröhlich, T.; Theska, R. On Modeling the Bending Stiffness of Thin Semi-Circular Flexure Hinges for Precision Applications. *Actuators*, 2018, 7(4), 86. https://doi.org/10.3390/act7040086
25. Xu, Q. Micromachines for Biological Micromanipulation. *Springer Cham*, 2018. ISBN: 978-3-319-74620-3.

26. Pan, P; Wang, W.; Ru, C.; Sun, Y.; Liu, X., MEMS-based platforms for mechanical manipulation and characterization of cells *J. Micromech. Microeng*., 2017, 27-123003.
27. Udvardi, P. et al., Spiral-Shaped Piezoelectric MEMS Cantilever Array for Fully Implantable Hearing Systems. *Micromachines*, 2017, 8(10),311. https://doi.org/10.3390/mi8100311
28. Abdalla, M. et al., Design of a piezoelectric actuator and compliant mechanism combination for maximum energy efficiency, *Smart Mater. Struct*., 2005, 14-1421.
29. Wei, H.; Shirinzadeh, B.; Li, W.; Clark, L.; Pinskier, J.; Wang, Y. Development of Piezo-Driven Compliant Bridge Mechanisms: General Analytical Equations and Optimization of Displacement Amplification. *Micromachines*, 2017, 8(8), 238. https://doi.org/10.3390/mi8080238
30. Pfusterschmied, G. et al.,Potential of Piezoelectric MEMS Resonators for Grape Must Fermentation Monitoring. *Micromachines*, 2017, 8(7), 200; https://doi.org/10.3390/mi8070200
31. Iandiorio, C; Salvini, P., Heavy Elastica soil-supported with lifting load and bending moment applied to an end: A new analytical approach for very large displacements and experimental validation, *International Journal of Solids and Structures*, 2020, 206, 153-169. https://doi.org/10.1016/j.ijsolstr.2020.09.014
32. Marotta, E.; Iandiorio, C; Salvini, P., Experimental setup for the evaluation of large displacements in the inflected beams sustained to ground, IOP Conf. Ser.: Mater. Sci. Eng., 2021, 1038-012078. doi:10.1088/1757-899X/1038/1/012078
33. Iandiorio, C; Salvini, P., Inflectional Heavy Elastica with Unilateral Contact constraint: Analytical Solution through the Curvilinear Abscissa Mapping approximation, *International Journal of Solids and Structures*, 2022, 234–235,111258. https://doi.org/10.1016/j.ijsolstr.2021.111258
34. De Bona, F.; Zelenika, S., A generalized elastica-type approach to the analysis of large displacements of spring-strips, *Proceedings of the Institution of Mechanical Engineers Part C Journal of Mechanical Engineering Science*, 1997, 211(7), 509-517.
35. Ahuett-Garza, H.; Chaides, O.; Garcia, P.N.; Urbina, P., Studies about the use of semicircular beams as hinges in large deflection planar compliant mechanisms, *Precision Engineering*, 2014, 38(4), 711-727. https://doi.org/10.1016/j.precisioneng.2014.03.008
36. Linß, S., Gräser, P.; Räder, T.; Henning, S.; Theska, R.; Zentner, L., Influence of geometric scaling on the elasto-kinematic properties of flexure hinges and compliant mechanisms, *Mechanism and Machine Theory*, 2018, 125, 220-239.
37. Henning, S., Linß, S.; Gräser, P.; Theska, R.; Zentner, L., Non-linear analytical modeling of planar compliant mechanisms, *Mechanism and Machine Theory*, 2021, 155,104067.
38. Valentini, P.P.; Pennestrì, E., Compliant four-bar linkage synthesis with second-order flexure hinge approximation, *Mechanism and Machine Theory*, 2018, 128, 225-233.
39. Valentini, P.P.; Cirelli, M.; Di Donato, S.; The compliant centrifugal pendulum as the vibration absorber with second-order elasto-kinematic approximation, *Journal of Vibration and Control Volume*, 2021, 27, 11-12, 1370 – 1381.
40. Valentini, P.P.; Pennestrì, E., Second-order approximation pseudo-rigid model of leaf flexure hinge, *Mechanism and Machine Theory*, 2017, 116, 352-359.
41. Cera, M.; Cirelli, M., Colaiacovo, L.; Valentini, P.P., Second-order approximation pseudo-rigid model of circular arc flexure hinge, *Mechanism and Machine Theory*, 2022, 175, 104963.
42. Valentini, P.P.; Cirelli, M.; Pennestrì, E., Second-order approximation pseudo-rigid model of flexure hinge with parabolic variable thickness, *Mechanism and Machine Theory*, 2019, 136, 178-189.
43. Šalinić, S.; Nikolic, A.V., A new pseudo-rigid-body model approach for modeling the quasi-static response of planar flexure-hinge mechanisms, *Mechanism and Machine Theory*, 2018, 124, 150-161.
44. Iandiorio, C; Salvini, P., An Analytical Solution for Large Displacements of End-Loaded Beams, *Proc. of the 1st Int. Conf. on Num. Mod. in Eng. NME, Lecture Notes in Mechanical Engineering*, 2018, Springer. https://doi.org/10.1007/978-981-13-2273-0_25
45. Iandiorio, C; Salvini, P., Large displacements of slender beams in plane: Analytical solution by means of a new hypergeometric function, *International Journal of Solids and Structures*, 2020, 185–186, 467-484. https://doi.org/10.1016/j.ijsolstr.2019.09.006
46. Batista, M., Analytical solution for large deflection of Reissner's beam on two supports subjected to central concentrated force, *International Journal of Mechanical Sciences*, 2016, 107, 13-20. doi.10.1016/j.ijmecsci.2016.01.002
47. Irschik, H.; Gerstmayr, J., A continuum mechanics based derivation of Reissner's large-displacement finite-strain beam theory: The case of plane deformations of originally straight Bernoulli-Euler beams, *Acta Mechanica*, 2009, 206(1), 1-21. doi.10.1007/s00707-008-0085-8
48. Timoshenko, S.P., Strength of Materials (Parts I & II), *David Van Nostrand Company*, 1940, New York.
49. Iandiorio, C; Salvini, P., An Engineering Theory of thick Curved Beams loaded in-plane and out-of-plane: 3D Stress Analysis, *European Journal of Mechanics - A/Solids*, 2022, 92, 104484. https://doi.org/10.1016/j.euromechsol.2021.104484
50. Lacarbonara, W., Nonlinear Structural Mechanics, Springer, 2013, New York. ISBN: 978-1-4419-1275-6
51. Rossi, A.; Botta, F. Optimised Voltage Distribution on Piezoelectric Actuators for Modal Excitations Damping in Tapered Beams. Actuators 2023, 12, 71. https://doi.org/10.3390/ act12020071
52. Thabuis, A.; Thomas, S.; Martinez, T.; Germano, P.; Perriard, Y., Designing compliant mechanisms composed of shape memory alloy and actuated by induction heating. *Smart Mater. Struct*., 2021, 30 095025.
53. Iandiorio, C; Salvini, P., Updated Lagrangian Curvilinear Beam Element for 2D Large Displacement Analysis, *Proc. of the 5st Int. Conf. on Num. Mod. in Eng. NME, Lecture Notes in Mechanical Engineering*, 2023, Springer.
54. Iandiorio, C; Salvini, P., Elastic-plastic analysis with pre-integrated beam finite element based on state diagrams: Elastic-perfectly plastic flow, *European Journal of Mechanics - A/Solids*, 2023, 97, 104837. https://doi.org/10.1016/j.euromechsol.2022.104837

55. Krause, M., Analysis der ebenen Bewegung, *Vereinigung Wissenschaftlicher Verleg*, 1920, Berlin.
56. Bottema, O., Some Remarks on theoretical Kinematics: Instantaneous Invariants, *Proceedings Intenrational Conference for Teachers of Mechanisms, The Shoe String Press*, 1961.
57. Veldkamp, G.R., Curvature Theory in Plane kinematics, Doctoral Dissertation, *J.B. Wolters Groningen*, 1963.
58. Woo, L.S.; Freudenstein, F., On the curves of synthesis in plane, instantaneous kinematics, *International Union of Theoretical and Applied Mechanics*, 1969, Springer, Berlin. https://doi.org/10.1007/978-3-642-85640-2_32
59. Di Benedetto, A.; Pennestrì, E., Introduzione alla Cinematica dei Meccanismi (vol.2), *Casa Editrice Ambrosiana*, 1993. ISBN: 8808084701
60. Roth, B.; Yang, A.T., Application of Instantaneous Invariants to the Analysis and Synthesis of Mechanisms, *J. Eng. Ind.*, 1977, 99(1), 97-103. https://doi.org/10.1115/1.3439172
61. Roth, B., On the advantages of instantaneous invariants and geometric kinematics, *Mechanism and Machine Theory*, 2015, 89, 5-13. https://doi.org/10.1016/j.mechmachtheory.2014.10.009
62. Figliolini, G.; Lanni, C., Geometric Loci for the Kinematic Analysis of Planar Mechanisms via the Instantaneous Geometric Invariants, *Mechanisms and Machine Science*, 2019, vol. 66., Springer, Cham. https://doi.org/10.1007/978-3-030-00365-4_22
63. Belfiore, N.P.; Simeone, P., Inverse kinetostatic analysis of compliant four-bar linkages, *Mechanism and Machine Theory*, 2013, 69, 350-372. doi.org/10.1016/j.mechmachtheory.2013.06.008
64. Luck, K.; Rehwald, W., Historical Evolution of the Pole-Theory. *International Symposium on History of Machines and Mechanisms*. Springer, 2004. https://doi.org/10.1007/1-4020-2204-2_25
65. Bresse, J.A.C., Memoire sur un theoreme nouveau concernant les mouvements plans, et sur l'application de la cinematique a la determination des rayons de courbure. *Journal de l'Ecole Polytechnique*, 1853, 35.
66. Beléndez, T.; Neipp, C.; Beléndez, A., An Integrated Project for Teaching the Post-Buckling of a Slender Cantilever Bar. *International Journal of Mechanical Engineering Education*, 2004, 32(1), 78 – 92. https://doi.org/10.7227/IJMEE.32.1.6